Journal of Applied Fluid Mechanics, Vol. 12, No. 4, pp. 1023-1035, 2019.
Available online at www.jafmonline.net, ISSN 1735-3645, EISSN 1735-3645.
DOI: 10.29252/jafm.12.04.29316

Channel Blockage and Flow Maldistribution during Unsteady Flow in a Model Microchannel Plate heat Exchanger

P. Dąbrowski†, M. Klugmann and D. Mikielewicz

Gdańsk University of Technology, Gdańsk, Pomorskie, 80-233, Poland

†*Corresponding Author Email: pawel.dabrowski@pg.edu.pl*

(Received June 27, 2018; accepted November 3, 2018)

ABSTRACT

This paper describes the problem of channel blockage as a result of flow maldistribution between the channels of a model mini channel plate heat exchanger consisting of one pass on each leg. Each leg of the heat exchanger contains 51 parallel and rectangular minichannels of four hydraulic diameters namely 461 µm, 571 µm, 750 µm and 823 µm. In addition, a more complex geometry has been investigated where for the sake of breaking the development length the inclined transverse cuts have been incorporated. The moment of liquid phase transition through the exchanger (the working medium: water) was recorded for the mass fluxes ranging from 18.67 to 277.76 kg/m2s in 51 parallel channels with the use of a fast speed camera. The Reynolds numbers Re in the individual channels were from 10.76 to 90.04. The relationship between the mass flux and the size of the minichannels in the presence of the maldistribution is discussed here. The existence of the threshold in the mass flux below which the phenomenon occurs has been shown. Two mechanisms of channel blocking have been recorded and described in detail. A miniscale variation of one of them containing the extended geometry was created as well.

Keywords: Minichannel; Minigeometries; Microgeometries; Transient state.

NOMENCLATURE

A	surface area
dh	hydraulic diameter
h	convective heat transfer coefficient
kf	thermal conductivity
m	mass flow rate
n	number of blocked channels
N	number of channels
Nu∝	Nusselt number for fully-developed temperature profile
Pw	wetted perimeter
Re	Reynolds number
Uc	velocity value in each microchannel
Um	mean value in microchannel velocities
x	absolute error
ΔP	pressure drop
Δx	measuring range
ρ	fluid density
σ	relative error
σU%	flow maldistribution factor

1. INTRODUCTION

All technology sectors are endeavoring to miniaturize products while simultaneously improving their performance. This causes the increase of heat flux which is necessary to dissipate from the surface. For example, the average value of heat flux for computer processors is from 2 to 4.5 MW/m^2 (up to 45 MW/m^2 in small areas); insulated gate bipolar transistors (IGBT) have average values from 6.5 to 50 MW/m^2. Poor thermal management is the main impediment to reach further miniaturization and well-known conventional and even compact heat exchangers have become insufficient in many cases. Hence, there is a need to focus on modern designs of highly compact and highly efficient heat exchangers in order to maximize the heat transfer rates. This is one of the reasons of the growing interest in heat transfer in micro-scale geometries (minichannels, minigaps) (Mikielewicz *et al.*, 2012). Attempts to apply such geometries to the development of highly efficient and compact heat

exchangers introduces a new quality but also involves specific problems just to mention: a) relatively high pressure drops, b) flow instabilities, c) maldistribution in individual channels, d) impact from fluid impurities that can easily block minichannels. Ensuring equal flow distribution between the minichannels is a fundamental problem which must be analyzed before proceeding with the most important issues from the application point of view - one and two-phase heat exchange. So, before starting to analyze the thermal efficiency of the exchanger, it must be certain that the operation is in the proper range of the flow parameters and that the entire exchanger structure works efficiently.

The hydraulic diameter can be calculated from Eq. (1) (Teng, 2012). Tuckerman and Pease (1981) clearly demonstrated, about four decades ago in Eq. (2), that the convective heat transfer coefficient strictly depends on the hydraulic diameter of the channel dh.

$$d_h = \frac{4A}{P_w} \tag{1}$$

The smaller the hydraulic diameter, the higher the convective heat transfer coefficient. This remark introduced a new generation of heat exchangers i.e. mini channel heat exchangers, in which laminar flows is recommended and the heat transfer coefficient is found from relation:

$$h = \frac{k_f Nu_\infty}{d_h} \tag{2}$$

Micro- and minichannels are different from the conventional channels in terms of channel hydraulic diameters. The ranges of hydraulic diameters proposed in (Mehendale *et al.*, 2000) are as follows: dh > 6 mm for macro channels, 1 mm < dh < 6 mm for compact channels, 0.1 mm < dh < 1 mm for meso channels and 1 μm < dh < 100 μm for micro channels. Different classifications were made in (Kandlikar and Grande, 2003) i.e. channels can be defined as: conventional when dh > 3 mm, mini when 0.2 mm < dh < 3 mm and micro when 10 μm < dh < 200 μm.

Mini- or microchannel heat exchangers are widely used in many industries: 1. the power industry (water cooled turbine blades, rocket nozzle cooling, fusion reactor blanket cooling, and domestic micro CHP) (Hall and Mudawar, 1999; Mikielewicz and Mikielewicz, 2010; Nacke *et al.*, 2011; Ornatskii and Vinyarskii, 1965; Sturgis and Mudawar, 1999), 2. the electronics industry (microprocessors, LED cooling) (Bahiraei and Heshmatian, 2017; Jajja *et al.*, 2014; Ramos-Alvarado *et al.*, 2013), 3. the avionics industry (avionics cooling) (Najim and Feddaoui, 2018), 4. the space industry (cooling of satellite electronics) (Brutin *et al.*, 2013), 5.the solar industry (solar, photovoltaic panels) (Robles *et al.*, 2014; Zhou *et al.*, 2017), 6. the automotive industry (multiport condensers) (Sakamatapan and Wongwises, 2014) , 7..the chemical and biological industry (Berthier *et al.*, 2015; JY *et al.*, 2015; P. Zhou *et al.*, 2017), 8.. the refrigeration industry (microfin tubes in residential cooling, heat pumps) (García-Cascales *et al.*, 2017; Illán-Gómez *et al.*, 2017) and 9. the cryogenic industry (heat exchangers for hydrogen production systems) (Zhou *et al.*, 2014). Kandlikar (2005) reports that microchannels may provide a heat flux dissipation ratio of up to 103 W/cm^2.

Small diameter channels cause a low mass flux of fluid that is able to flow through it and still result in a high heat flux that can be dissipated from a cooled surface. That provides an application for many parallel minichannels with common inlet and outlet manifolds in minichannel heat exchangers. However, this kind of construction induces a flow maldistribution. According to (Mueller and Chiou, 1988), the prefix "mal" means defective or bad. Thus, if a comparison is made to a uniform distribution, then "maldistribution" means unequal amounts of fluid or unequal flow velocity in each channel. In fact, there are two kinds of maldistribution connected with fabrication conditions:1. gross maldistribution and 2. passage-to-passage maldistribution (Wen and Li, 2004). The first one is associated with mechanical design issues mainly due to improper header configuration, and the second one is caused by various manufacturing tolerances. However, flow maldistribution can also appear due to the heat transfer process, two-phase flows and fouling or corrosion (Mueller and Chiou, 1988).

A very significant part of designing of heat exchanger is to choose proper inlet and outlet manifold configuration. Two main structures of manifolds can be distinguished: 1.consecutive and 2. bifurcation (Wang, 2011). They are shown in Fig. 1 (Amador *et al.*, 2004). Moreover, the typical flow configurations for minichannel plate heat exchangers are shown in Fig. 2 (Kumar *et al.*, 2017).

In consecutive manifolds the main fluid stream is divided continuously into channels as it reaches them. This structure is very common due to their simplicity and lower pressure drop compared to the bifurcation type. However, consecutive manifold is susceptible to flow maldistribution. The bifurcation structure is inspired by nature and can be seen in trees, cracks in dry ground, the blood circulation system and lungs (Bejan and Errera, 1997). Here the main fluid stream is divided into two streams; each stream is then further subdivided into two more until the number of divisions matches the number of channels. They then merge until the creation of the main fluid stream. In paper (Mu *et al.*, 2015), comparisons of some flow fields were made, and it was determined that the bifurcation structure (the circular turning constructal distributor) gives excellent distribution, which resulted in a very uniform temperature field over the heating surface.

Many authors have conducted experiments that have specified parameters affecting flow distribution. Minqiang *et al.* (2009) carried out CFD-based studies of maldistribution in 20 parallel channels. The variable parameters were manifold's dimensions (length, magnitude and position of inlet/outlet) and microchannels' dimensions (length, width and depth). All these parameters influence distribution in

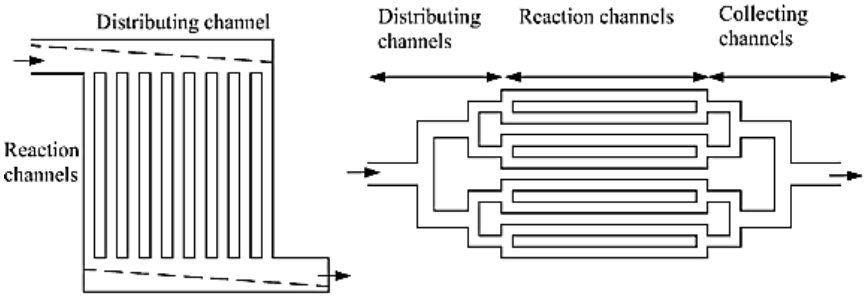

Fig. 1. Schematic for consecutive (left) and bifurcation (right) manifold of minichannel heat exchangers (Amador *et al.*, 2004).

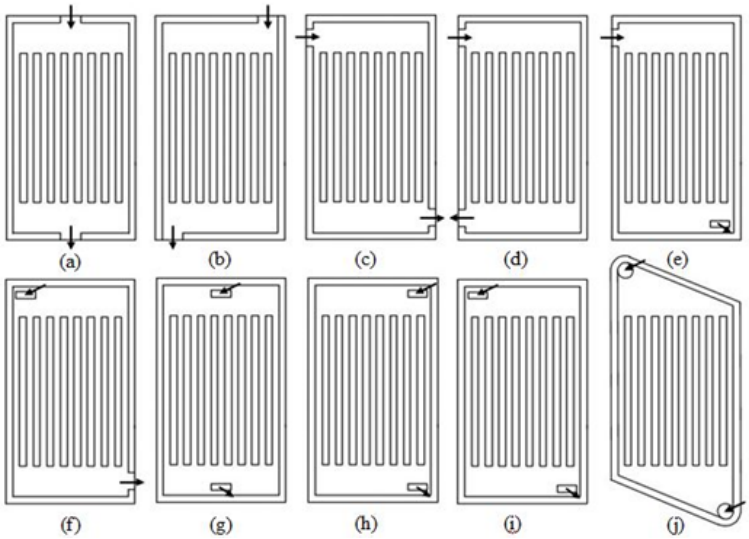

Fig. 2. Flow configurations reported in literature: (a) I type (b) N type (c) Z type (d) D type (e) L type (f) L` type (g) U type (h) U′ type (i) V type (j) V′ type (Kumar *et al.*, 2017).

channels. Kumaraguruparan *et al.* (2011) conducted numerical and experimental research of flow maldistribution in parallel microchannels in a U-type configuration. These studies show the presence of flow separation, backflows and a vortex at the inlet. These phenomena cause maldistribution but the increase in viscosity of the fluid reduces these effects. Another research project on the influence of flow maldistribution on temperature distribution and hot spot formation in 10 parallel channels with various hydraulic diameters was carried out on (Manoj Siva *et al.*, 2014). The authors investigated and compared maldistribution on three channel flow configurations (U, Z, I-type) and the various heat flux generated. They found out that the smaller the diameter of channels, the smaller the maldistribution. Thus, the temperature difference over the surface was also smaller. Other researchers (Anbumeenakshi and Thansekhar, 2016) found out that the best distribution is obtained when the fluid enters the inlet header perpendicular to the length of the header. Moreover the rectangular header shape gives lower maldistribution at a high flow rate while the trapezoidal and triangular header shape gives lower maldistribution at a low flow rate. It is found that, irrespectively of header shape or flow inlet configuration, the flow becomes more uniform at a higher flow rate.

There are many ways of presenting the maldistribution phenomenon as a quantitative effect. Different authors define it in different ways choosing various parameters as a representative value. Minqiang *et al.* (2009) define maldistribution with the parameter σU% set as follows:

$$\sigma_{U\%} = \sqrt{\frac{1}{N}\sum_{i=1}^{N}\left(\frac{U_{C(i)}}{U_m} - 1\right)^2}\; x100 \tag{3}$$

Where Uc(i) is the velocity value of each microchannel, Um is the mean value of microchannel velocities, defined as:

$$U_m = \frac{1}{N}\sum_{i=1}^{N} U_{c(i)} (i = 1,2,...,N) \tag{4}$$

Hence, one way to represent the distribution in a microchannel heat exchanger is to measure the fluid velocity in every one of the N channels and refer those values to the mean value of the flow velocity in the whole device.

The purpose of the presented research was to find the relationship between the flowrate and the hydraulic

diameter of minichannels and the onset of the maldistribution phenomena. A single exchanger's plate containing 51 parallel and rectangular minichannels of hydraulic diameters 461 μm, 571 μm, 750 μm and 823 μm was subject to analysis. These plates were designed and investigated in other aspects earlier (Mikielewicz and Wajs, 2017; Wajs *et al.*, 2016). In addition, the more complex geometry, equipped with additional diagonal channels (so called extended geometry) has been investigated. The conditions were adiabatic. The analysis was related to the moment of the liquid phase transition through the measurement section with the use of water as a working medium. This process was registered with a fast shutter speed camera and designated recording software.

2. EXPERIMENTAL SETUP AND RESEARCH PROCEDURE

The measuring system was built as an open loop. Demineralized and degassed water was supplied to the installation gravitationally using a miniature water tower where hydrostatic pressure was produced in sufficient amount to provide inlet parameters to the test section. Its design (hydrostatic pressure, cross-sections of pipelines) was established to provide a pressure of 5 kPa and up to 16.6 g/s of flowrate at the inlet to the test section. The range of flow parameters for which the measurements were carried out were directly matched with the nature of thermosiphon's work which is envisaged as a subsequent stage of works on the implementation of that geometry of the heat exchanger in the solar assisted installation. The diagram of the experimental rig is shown in Fig. 3.

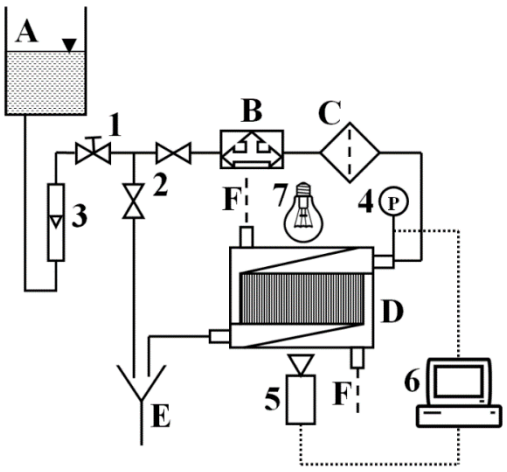

Fig. 3. Diagram of experimental rig; elements of the flow system: A – water tank, B – air separation system, C – filter, D – test section, E – outflow, F – section heating/cooling facility; elements of the control and measuring system: 1 – control valve, 2 – cut-off valve, 3 – rotameter, 4 – pressure transducer, 5 – fast shutter speed camera, 6 – synchronization and data acquisition system, 7 – light source.

A conventional digital camera was used to record the fluid distribution in the test section. The camera allows sequences to be recorded at 1920x1080 (FullHD) resolution. Other parameters: shutter speed of 50 ÷ 500 μs, frame rate of 50 fps, and focal length (small pic. eqiv.) = 70 mm. The traditional 1000 W halogen lamp was used to illuminate the measuring section.

Pressure measurements were carried out using an ATM.1ST electronic pressure transmitter with a measuring range of 0 ÷ 5 kPa. It cooperates with a National Instruments SCXI-1600 measuring interface and LabVIEW environment. A volumetric flowrate measurement was accomplished using a rotameter with a measuring range of 0 ÷ 8.33 cm^3/s and the elementary scale equal to 0.083 cm^3/s. The mass flow rate was then calculated as well as the mass flux.

In addition, the measurement system was equipped with the de-aeration facility and a filter to remove any unwanted inclusions in the tested liquid.

The following geometries were investigated:

- basic (Fig. 4), consisting of 51 parallel minichannels, width 1 mm, depth 0.3 mm (461 μm), 0.4 mm (571 μm), 0.6 mm (750 μm) and 0.7 mm (823 μm),
- extended (Fig. 5), consisting of 51 parallel minichannels with additional cross-cut channels, width 1 mm, depth 0.4 mm (461 μm).

As can be seen in Fig. 4 and Fig. 5, investigations are concerned with the inlet and outlet triangular collectors.

The experiment was performed at flowrates ranging from 0.83 g/s to 8.33 g/s and, for some cases, additionally at 10 g/s and 13.33 g/s to accurately register the specifics of the pressure drop. No channel blocking phenomena were observed for the flowrate above 8.33 g/s, so there was no need to extend the measurements above this value for all cases. The Reynolds number in the individual channel considered in this work ranges from 10.76 to 90.04. The pressure measurement was done only at the inlet. The atmospheric pressure was assumed at the outlet. The geometry of the V'-type has been selected as the one exhibiting least maldistribution.

3. RESULTS AND DISCUSSION

3.1 Flow Maldistribution

Repeatable results have been obtained. That is clearly seen in Fig. 6. The shape of the flow profile is caused by the geometry of the test section i.e. the shape and dimensions of the inlet and outlet manifold and the cross-sections of the minichannels. Figure 6 shows also a phenomenon of flow maldistribution. The front of the flow in every single channel is not collinear and has a different velocity, i.e. channels are filled out at different times. It was observed that the flow maldistribution depends on the volumetric flow rate (higher flow rate, more uniform distribution) and the hydraulic diameter of the

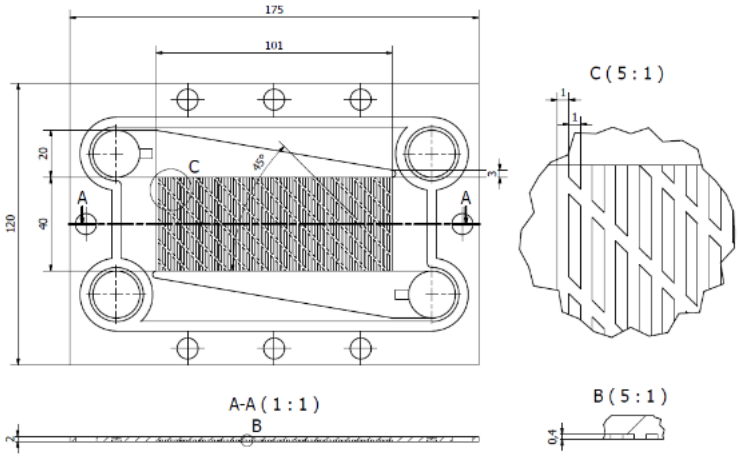

Fig. 5. The investigated extended minichannel plate.

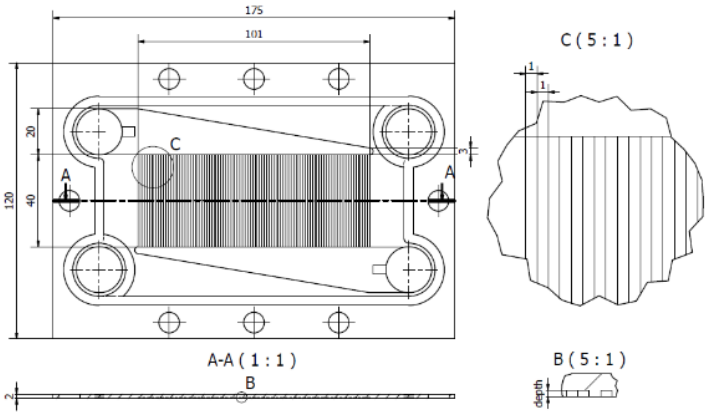

Fig. 4. The investigated basic minichannel plate0.

channels (lower hydraulic diameter, more uniform distribution). It corresponds with many authors' observations that in order to reduce the flow maldistribution, the effect of inertia should be reduced and the effect of viscosity should be increased. Then the larger pressure drop should be in the channels and the lower pressure drop in the inlet and outlet manifolds (Anbumeenakshi and Thansekhar, 2016; Kumaraguruparan et al., 2011; Tuo and Hrnjak, 2013).

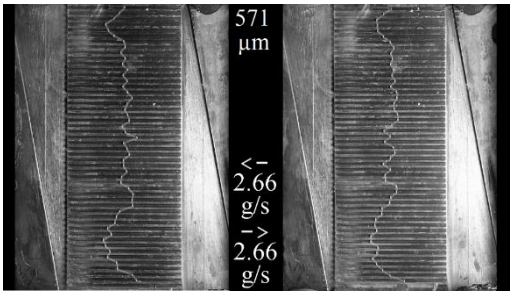

Fig. 6. Comparison of flow profiles for two different measurement series concerning the same minichannel hydraulic diameter (571 µm) at equal mass flow rates of 2.66 g/s.

Most of the studies are made in the steady state, e.g. at a constant flow rate and at a constant temperature or constant heat flux. Every installation has to be started up at least once, but in many cases the moment when the working fluid starts to flow occurs periodically. Current studies show the moment when the liquid phase enters the model minichannel heat exchanger. This approach allowed for the observation of the phenomena of channel blockage, which, to the best of the authors' knowledge, had not been described yet.

The test section (geometry with hydraulic diameter of 750 μm) where the front of flow reached the outlet at different flow rates is presented in Fig. 7. The white lines represent the blocked channels that were not filled with the liquid phase entirely. The black lines represent the blocked channels filled with water but blocked with a gaseous bubble in the outlet manifold. The working fluid does not flow in the channels that are not filled with the working medium entirely, so the heat exchanger works unevenly. In practice, the uneven temperature distribution over the surface and lower heat exchanger's efficiency should be observed due to this situation. It was seen that more minichannels are inactive at low flow rates. The amount of inactive channels at the lowest flow rate (1 g/s) is 16 and for 3.5 g/s, 6.16 g/s, 8.16 g/s the

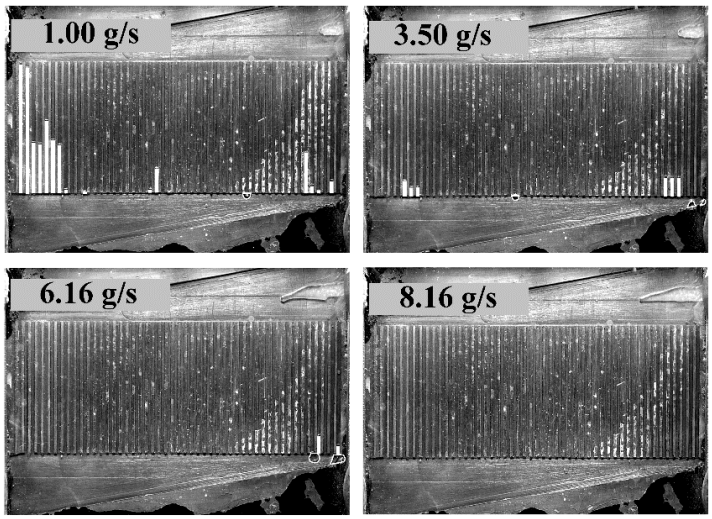

Fig. 7. View of the test section with blocked channels at different flow rates in the same geometry (minichannel hydraulic diameter of 750 µm).

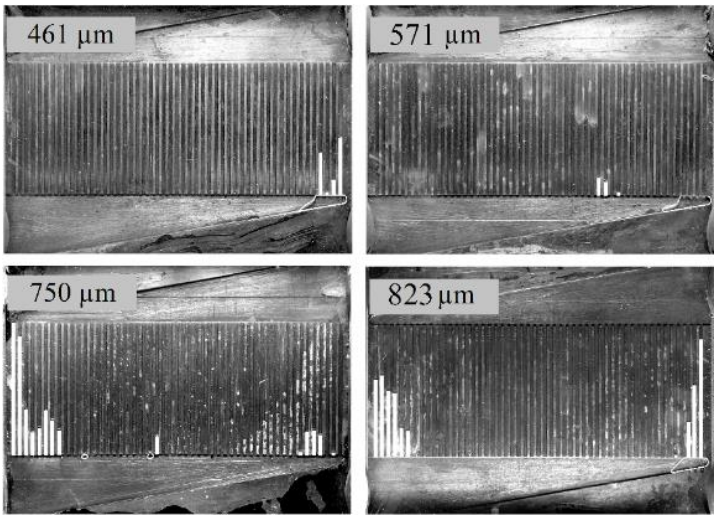

Fig. 8. View of the test section with blocked channels in different geometries (minichannel hydraulic diameter of 461 µm ÷ 823 µm) at the same flow rate of 1.83 g/s.

amount becomes smaller (7, 3 and 0 respectively). It is clearly shown that such low flow rates should be avoided.

The test section is in a similar situation as before, but this time the channel depth is a varying parameter and the flow rate in every case is the same and equals to 1.83 g/s, which is just like what is presented in Fig. 8. It is seen that a bigger hydraulic diameter of channels causes more channels to be inactive (see Fig. 9). This amount rises from 4 inactive channels for the 461 µm hydraulic diameter to 16 inactive channels for the 823 µm hydraulic diameter. For the 571 µm and 750 µm minichannel hydraulic diameters, the amount of inactive channels are 7 and 10, respectively. It can be deduced that the channels are blocked with a recurrent mechanism that is strictly connected to flow maldistribution. For every geometry (for every size of minichannel), there is a certain critical flowrate at which the inactive channels start to appear. Then, the number of inactive channels increases in proportion to the further reduction of the flowrate.

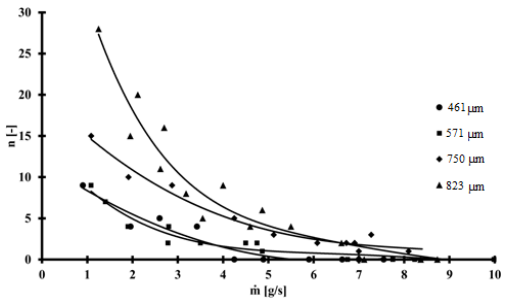

Fig. 9. The number of permanently blocked channels as a function of the mass flowrate for several minichannel depths.

The analysis of the images was done to calculate the velocity in every single channel. As mentioned before, the flow distribution was recorded at 50 fps. It gives a single frame in the interval of time of 0.02 s. The total length of a single channel was 400 mm. The frame corresponding to the moment where water starts to enter the channel and the frame where water exits gives information about the total the time required to flow through the channel. It enables to calculate the velocity in every single channel. The velocity in the blocked channels is assumed as 0 m/s, which appears as a gap in the charts. The channel number 1 was the first channel, near to the inlet and channel number 51 was the last channel, near to the outlet. The mean velocity in the particular channel Um was calculated from Eq. (4), where N was taken as a number of active (not blocked) channels. The values of the velocities have been non-dimensionalised by dividing the actual values in the channel against the value of the velocity resulting from the even distribution in the channels.

Figure 10 shows a generalized case - the number of blocked channels in the function of mass flux G. There is a visible trend towards the disappearance of the channel blocking the phenomenon as the mass flux increases.

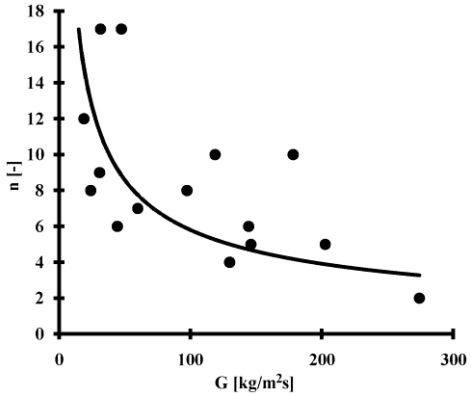

Fig. 10. Number of permanent blocked channels as a function of mass flux.

A similar trend can be seen in Fig. 11, showing the dependence of the maldistribution coefficient (σU%) on the mass flux. The maldistribution coefficient was calculated from Eq. (3). A higher maldistribution coefficient means a higher difference in velocity between channels. It is clearly seen that low mass fluxes result in higher flow maldistribution which corresponds also to a greater number of blocked channels.

In Figs. 12 ÷ 15 is shown the non-dimensional fluid velocity distribution in individual channels for various mass fluxes for four hydraulic diameters 461 μm, 571 μm, 750 μm and 823 μm, respectively. It is clearly seen that the fluid velocity distribution is closer to the expected (Uc/Um closer to 1) for the higher hydraulic diameters. Simultaneously, regardless of the hydraulic diameter more uniform fluid distribution is obtained for higher mass fluxes. This is summarized in Fig. 16.

Although the non-dimensional fluid velocity distribution for similar mass fluxes is alike, a higher hydraulic diameter causes more blocked channels. This is shown in Fig. 17. Blocked channels appear mainly close to the inlet and close to the outlet.

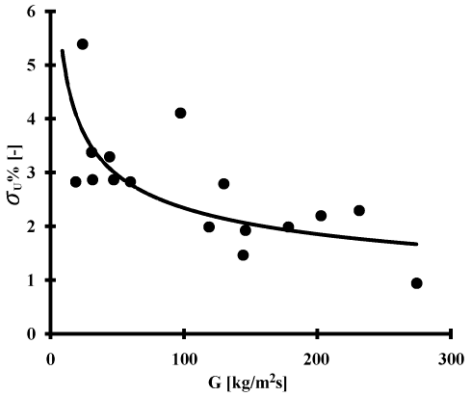

Fig. 11 Maldistribution coefficient as a function of mass flux.

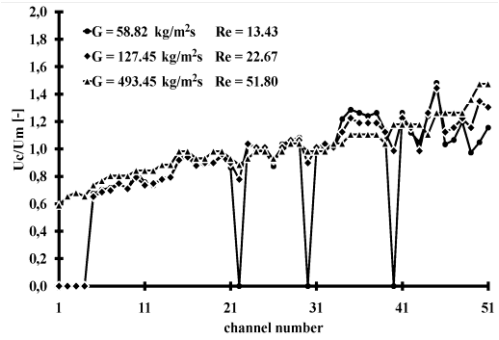

Fig. 12. Non-dimensional fluid velocity distribution in individual channels for various mass fluxes; dh=461 µm.

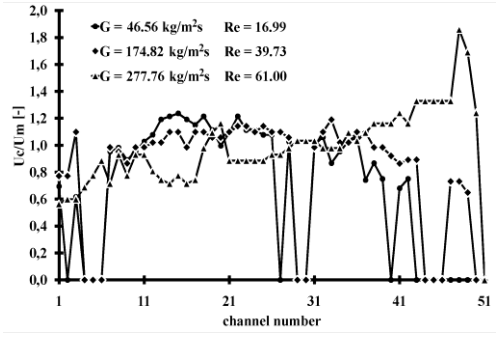

Fig. 13. Non-dimensional fluid velocity distribution in individual channels for various mass fluxes; dh=571 µm.

3.2 Mechanisms of Channel Blocking

In general, the channel blocking mechanisms are a derivative of the flow maldistribution. Based on the research carried out, it is clear that the quality of the whole system is dependent on the flowrate of the tested fluid.

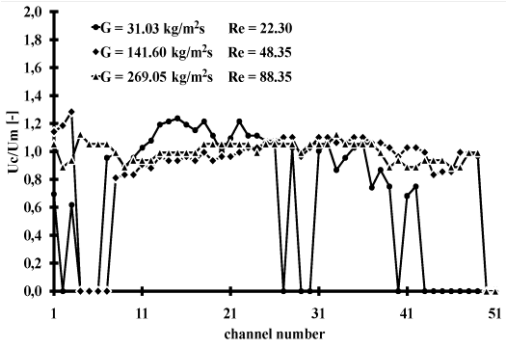

Fig. 14. Non-dimensional fluid velocity distribution in individual channels for various mass fluxes; dh=750 µm.

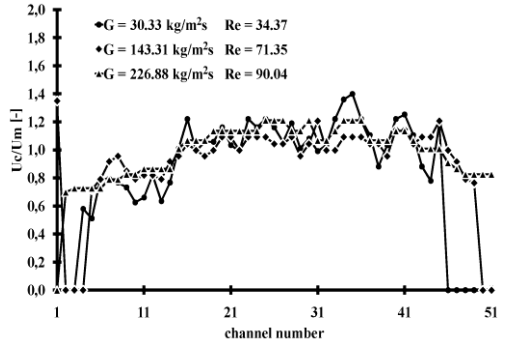

Fig. 15. Non-dimensional fluid velocity distribution in individual channels for various mass fluxes; dh=823 µm.

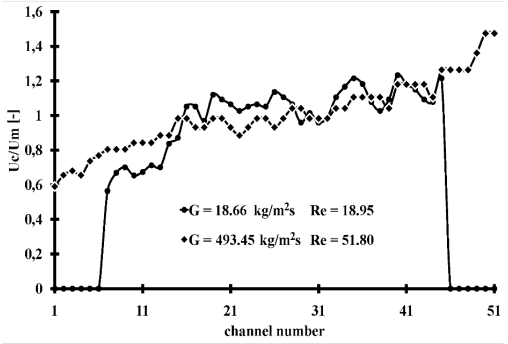

Fig. 16. Non-dimensional fluid velocity distribution in individual channels for lowest and highest mass flux.

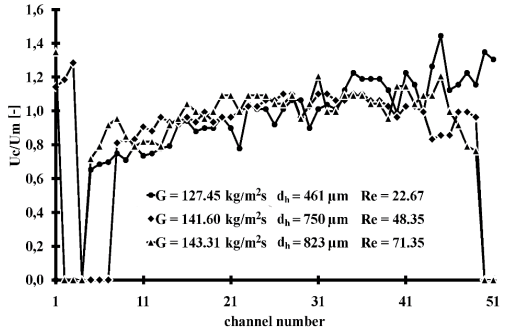

Fig. 17. Non-dimensional fluid velocity distribution in individual channels for various hydraulic diameters and similar mass fluxes.

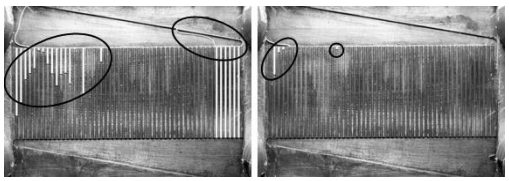

Fig. 18. Plate with minichannels of 571 µm hydraulic diameter; left: flowrate 1.26 g/s, the numerous inactive channels and the large bubble in the outlet manifold can be seen; right: flowrate 3.73 g/s, only a few inactive channels and no large bubble.

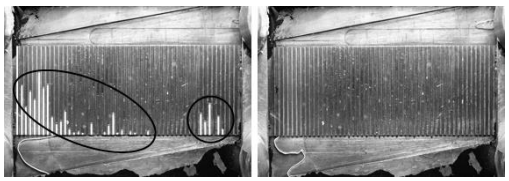

Fig. 19. Plate with minichannels of 750 µm hydraulic diameter; left: flowrate 1.25 g/s, numerous inactive channels; right: flowrate 13.33 g/s, no inactive channels.

The overall maldistribution mechanism is following. This occurs in places where a trapped bubble of gas phase is encountered and is cut off by the liquid phase (Fig. 18 and Fig. 19). Typically, this refers to those channels where the medium also previously flowed from the inlet manifold. As can be seen in Fig. 20 and Fig. 21, two typical repetitive mechanisms can be identified in the specific flow system of the measuring section, namely the mechanism denoted as 1 and 2, described on further.

Mechanism type 1 (seen in Fig. 20) is based on the blocking of lateral minichannels through a large bubble of gas phase which is trapped in the narrowest part of an outlet manifold. In these channels, an outflow is delayed in relation to the center of the section and it continues until the moment when the medium draining from the channels closer to the center fills the entire width of the outlet manifold. Then, the bubble is getting blocked and has no way to leave the collector. The channels within its reach remain inactive with the lateral part of the collector. The flow takes place in the remaining part of it. Despite the identical configuration of inlet and outlet manifolds, this mechanism has not been observed for all cases (minichannel depths).

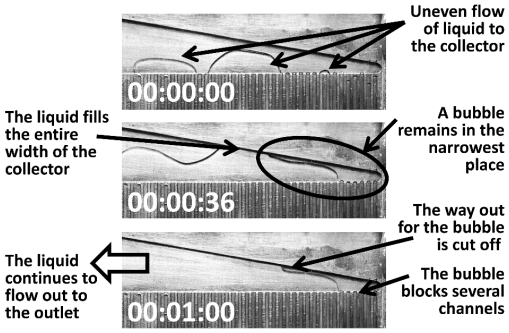

Fig. 20. Channel blocking - type 1, a part of the phenomenon with a duration of 1 second.

Mechanism type 2 (seen in Fig. 21) consists of cutting off bubbles of gas phase in individual channels through a forward flow of liquid phase in the outlet manifold. As in the case of type 1, the phenomenon affects channels in which the flow has been delayed, but it can happen anywhere, not only on the border of the section. However, this phenomenon is most evident and occurs longest on the side of the section where the inlet manifold is narrowest (the opposite side to the location of mechanism type 1). Liquid leaving those channels that have been filled first fills the outlet manifold and forms the flow front. The flow front moves towards the outlet of the section. If it encounters a "delayed" channel with a bubble of gas phase inside, the bubble will get trapped. In some cases it is able to get out, but in most cases, it stays and blocks the channel.

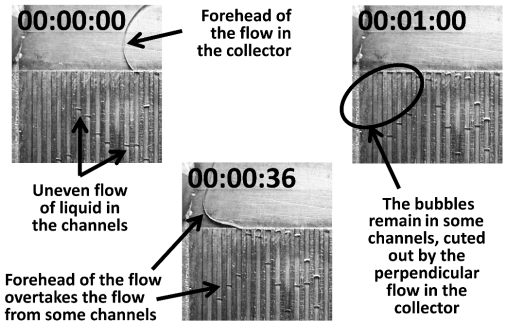

Fig. 21. Channel blocking - type 2, a part of the phenomenon with a duration of 1 second.

3.3 Case of Extended Geometry

In the extended geometry, both of the described phenomena are possible between the ends of the minichannels and the output manifold. However, mechanism type 2 may additionally occur wherever the "main" and transverse channels are intersected (Fig. 22). That is expected to contribute to boundary layer breakup. For this reason, providing optimum distribution of the medium in the extended geometry is a much more complicated issue.

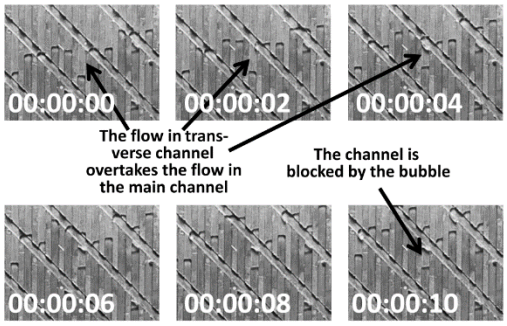

Fig. 22. Local channel blocking - type 2 in extended geometry, example 1, duration 0.10 second.

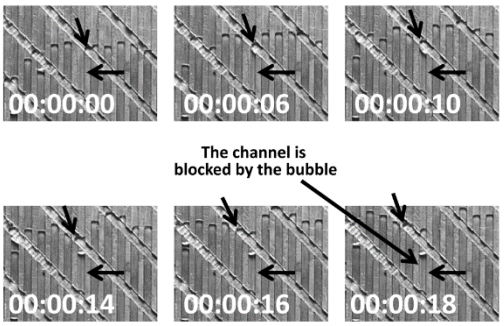

Fig. 23. Local channel blocking - type 2 in extended geometry, example 2, duration 0.18 second.

The occurrence of a third type of channel blocking process (running locally) as seen in Fig. 23, in addition to the phenomena known for basic geometry, causes such unambiguous logic that, as described above, it cannot be indicated in the extended geometry. Overlapping the three phenomena results in a complex situation, Fig. 24.

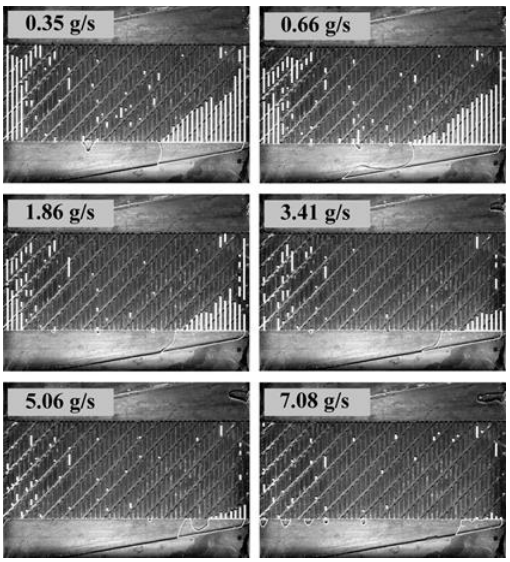

Fig. 24. Segments of permanent inactive channels for the plate of 571 μm hydraulic diameter, extended geometry, for different flowrates

As can be seen in Fig. 22 and Fig. 23, the test fluid has many optional routes. There are also many local conditions that change in a stochastic (or logical, but difficult to describe) way. Despite the trend to reduce the number of blocked channels, the blocking process occurs on a large scale. According to mechanism 1, this occurs up to a flowrate of 8.33 g/s. Meanwhile, for the basic geometry and for flowrates above 5 g/s, the maldistribution is not present at all (Fig. 25). Local blocking was observed up to a flow rate of 13.33 g/s for the extended geometry.

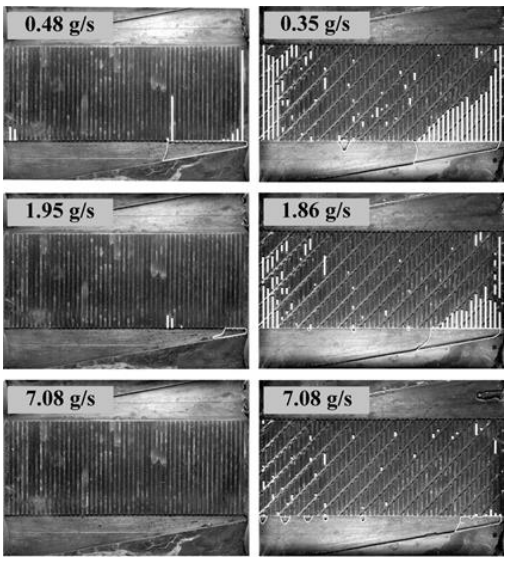

Fig. 25. Comparison of channel blocking for the corresponding geometries – 571 µm basic and 571 µm extended, and for similar flowrates.

3.4 Pressure drop

From the application perspective, the important information is the total pressure drop in the exchanger. This must take into account not only the inlet manifold, set of minichannels and the outlet manifold, but also the entire remaining flow system. The example of such an approach is shown in Fig. 26. In general, the pressure drop as a function of mass flow rate increases as the mass flow rate increases. This is in line with the currently accepted knowledge about the flow phenomena. The curves of the total pressure drop in the model exchanger are clearly parabolic, which means it is very strongly increasing for higher flowrate values.

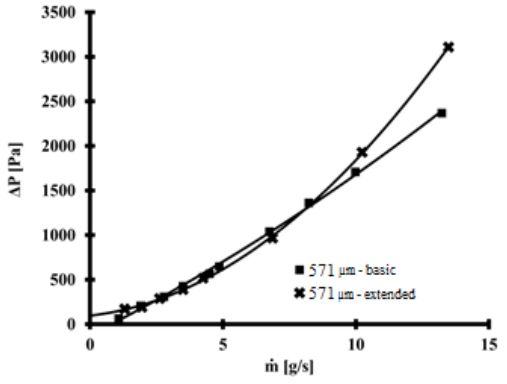

Fig. 26. Total pressure drop in the model exchanger (including inlet connector) as a function of mass flow rate for basic and extended geometry.

4. THE UNCERTAINTY ANALYSIS

Experimental uncertainty was determined using the sequential perturbation method of error analysis (Moffat, 1988). This method allows determining of the total experimental error by including errors originating from individual sources into the general database and averaging it using a root sum square method (RSS) (Eq. (5)).

$$RSS = \sqrt{\sum_{i}^{N} \sigma_{(i)}{}^{2}} \tag{5}$$

The relative error is defined by Eq. (6):

$$\sigma = \frac{\Delta x}{x} \tag{6}$$

where Δx is the absolute error and x is the measuring range.

According to this method, part of the measurements made using measuring instruments shows a relatively high accuracy and the resulting inaccuracies should not exceed 3.62%. A detailed list can be found in Table 1.

5. CONCLUSION

On the basis of the accomplished work the following conclusions can be drawn.

a. Comprehensive experimental studies enabled the recognition of the maldistribution mechanism in the minichannel geometry and its dependence on the main parameters such as minichannel size and flowrate. The impact of the extended geometry was also observed. It has been noticed that there is a critical flow rate below which the distribution of the liquid between the minichannels worsens. The number of inactive channels increases with a further decrease in the flow rate as well as a decrease in the Reynolds number. The critical flow rate depends on the specific geometry.

b. Flow visualization has helped to register two types of characteristic and fully repetitive channel blocking mechanisms. In the case of the basic geometry, channel blocking could only occur between the end of the channels and the outlet collector. In the case of the extended geometry, this phenomenon is possible wherever the "main" and transverse channels are intersected. For this reason providing optimum distribution of the fluid in the extended geometry seems to be much more difficult.

c. The increase in the flow resistance and the pressure drop for the increasing flow rates has been confirmed. This increase follows the parabolic distribution. The application of more complicated geometry causes a further increase in the flow resistance at higher flow rates (above 8.33 g/s). The possible reason for this can be the flow turbulence.

d. Due to the critical flow rate below which the deterioration of the operation occurs and the parabolic nature of the pressure drop curve, there is a narrow range of flow rates at which model geometries can work optimally. It is a range in the order of 5 g/s to 8.33 g/s. In this range the pressure drops are in the range of 600

Table 1 Partial experimental uncertainties

Measured number	Measuring range	Absolute error	Relative error
Flow position in single channel	40 mm	0.07 mm	0.18%
Flow velocity in single channel (low flows, about 1 g/s)	40 mm/s	0.53 mm/s	1.32%
Flow velocity in single channel (high flows, about 8 g/s)	125 mm/s	2.66 mm/s	2.13%
Inlet pressure	5 kPa	10 Pa	0.20%
Total mass flowrate	8.33 g/s	0.086 g/s	1.16%
Hydraulic channel diameter	823 µm	0.05 mm	2.33%

Pa ÷ 1250 Pa, depending on the hydraulic diameter of the channels. These values seem to be appropriate for the intended use of the assumed geometry in a solar thermosiphon installation.

e. The proposed experimental method allows to legibly locate the weak points of the flow system. The authors assume that the observations will remain valid for other cases, such as two-phase mixtures or boiling flows.

ACKNOWLEDGEMENTS

The work presented in this paper was funded from the National Science Centre, Poland research project No. 2017/27/N/ST8/02785 in the years 2018-2020, the National Science Centre, Poland research project No. 2015/19/D/ST8/03201 in the years 2016–2019 and partially from the project DST/INT/Pol/P-29/2016 (third author).

REFERENCES

Amador, C., A. Gavriilidis and P. Angeli (2004). Flow Distribution in Different Microreactor Scale-out Geometries and the Effect of Manufacturing Tolerances and Channel Blockage. *Chemical Engineering Journal* 101(1–3), 379–90.

Anbumeenakshi, C. and M. R. Thansekhar (2016). Experimental Investigation of Header Shape and Inlet Configuration on Flow Maldistribution in Microchannel. *Experimental Thermal and Fluid Science* 75, 156–61.

Bahiraei, M. and S. Heshmatian. (2017). Application of a Novel Biological Nanofluid in a Liquid Block Heat Sink for Cooling of an Electronic Processor: Thermal Performance and Irreversibility Considerations. *Energy Conversion and Management* 149, 155–67.

Bejan, A. and M. R. Errera. (1997). Deterministic Tree Networks for Fluid Flow: Geometry for Minimal Flow Resistance Between a Volume and One Point. *Fractals* 5(4), 685–95.

Berthier, J., K. A. Brakke, E. P. Furlani, I. H. Karampelas, V. Poher, D. Gosselin, M. Cubizolles and P. Pouteau. (2015). Whole Blood Spontaneous Capillary Flow in Narrow V-Groove Microchannels. *Sensors and Actuators, B: Chemical* 206, 258–67.

Brutin, D., V. S. Ajaev and L. Tadrist (2013). Pressure Drop and Void Fraction during Flow Boiling in Rectangular Minichannels in Weightlessness. *Applied Thermal Engineering* 51(1–2), 1317–27.

García-Cascales, J. R., F. Illán-Gómez, F. Hidalgo-Mompeán, F. A. Ramírez-Rivera and M. A. Ramírez-Basalo (2017). Performance Comparison of an Air/Water Heat Pump Using a Minichannel Coil as Evaporator in Replacement of a Fin-and-Tube Heat Exchanger. *International Journal of Refrigeration* 74, 558–73.

Hall, D., and I. Mudawar. (1999). Ultra-High Critical Heat Flux (CHF) for Subcooled Water Flow Boiling?II: High-CHF Database and Design Equations. *International Journal of Heat and Mass Transfer* 42(8), 1429–56.

Illán-Gómez, F., J. R. García-Cascales, F. Hidalgo-Mompeán and A. López-Belchí (2017). Experimental Assessment of the Replacement of a Conventional Fin-and-Tube Condenser by a Minichannel Heat Exchanger in an Air/Water Chiller for Residential Air Conditioning. *Energy and Buildings* 144, 104–16.

Jajja, S. A., W. Ali, H. M. Ali and A. M. Ali. (2014). Water Cooled Minichannel Heat Sinks for Microprocessor Cooling: Effect of Fin Spacing. *Applied Thermal Engineering* 64(1–2), 76–82.

Kandlikar, S. G. (2005). High Flux Heat Removal with Microchannels—A Roadmap of Challenges and Opportunities. *Heat Transfer Engineering* 26(8), 5–14.

Kandlikar, S. G., and W. J. Grande. (2003). Evolution of Microchannel Flow Passages--Thermohydraulic Performance and Fabrication Technology. *Heat Transfer Engineering* 24(1), 3–17.

Kumar, R., G. Singh, and D. Mikielewicz. (2017). A New Approach for the Mitigating of Flow Maldistribution in Parallel Microchannel Heat Sink. *Journal of Heat Transfer (c).*

Kumaraguruparan, G., R. Manikanda Kumaran, T. Sornakumar and T. Sundararajan. (2011). A Numerical and Experimental Investigation of Flow Maldistribution in a Micro-Channel Heat Sink. *International Communications in Heat*

and Mass Transfer 38(10), 1349–53.

Siva, M. V., A. Pattamatta and S. K. Das. (2014). Effect of Flow Maldistribution on the Thermal Performance of Parallel Microchannel Cooling Systems. *International Journal of Heat and Mass Transfer* 73, 424–28.

Mehendale, S. S., A. M. Jacobi and R. K. Shah (2000). Fluid Flow and Heat Transfer at Micro- and Meso-Scales With Application to Heat Exchanger Design. *Applied Mechanics Reviews* 53(7), 175–93.

Mikielewicz, D. and J. Wajs (2017). Possibilities of Heat Transfer Augmentation in Heat Exchangers with Minichannels for Marine Applications. *Polish Maritime Research* 24(s1), 133–40.

Mikielewicz, D. and J. Mikielewicz. (2010). A Thermodynamic Criterion for Selection of Working Fluid for Subcritical and Supercritical Domestic Micro CHP. *Applied Thermal Engineering* 30(16), 2357–62.

Mikielewicz, D., M. Klugmann and J. Wajs (2012). Experimental Investigation of M-Shape Heat Transfer Coefficient Distribution of R123 Flow Boiling in Small-Diameter Tubes. *Heat Transfer Engineering* 33(7), 584–95.

Minqiang, P., Z. Dehuai, T. Yong and C. Dongqing (2009). CFD-Based Study of Velocity Distribution among Multiple Parallel Microchannels. *Journal of Computers* 4(11), 1133–38.

Moffat, R. J. (1988). Describing the Uncertainties in Experimental Results. *Experimental Thermal and Fluid Science* 1(1), 3–17.

Mu, Y. T., L. Chen, Y. Ling He, and W. Quan Tao. (2015). Numerical Study on Temperature Uniformity in a Novel Mini-Channel Heat Sink with Different Flow Field Configurations. *International Journal of Heat and Mass Transfer* 85, 147–57.

Mueller, A. C. and J. P. Chiou. (1988). Review of Various Types of Flow Maldistribution in Heat Exchangers. Heat Transfer Engineering 9(2), 36-50.

Nacke, R., B. Northcutt, and I. Mudawar. (2011). Theory and Experimental Validation of Cross-Flow Micro-Channel Heat Exchanger Module with Reference to High Mach Aircraft Gas Turbine Engines. *International Journal of Heat and Mass Transfer* 54(5–6), 1224–35.

Najim, M., and M. Barek Feddaoui. (2018). New Cooling Approach Using Successive Evaporation and Condensation of a Liquid Film inside a Vertical Mini-Channel. *International Journal of Heat and Mass Transfer* 122, 895–912.

Ornatskii, A. P. and L. S. Vinyarskii (1965). Heat Transfer Crisis in a Forced Flow of Underheated Water in Small-Bore Tubes. *Teplofizika Vysokikh Temperatur* 3(1965): 441–51.

Ramos-Alvarado, B., Bo F. and G. P. Peterson. (2013). Comparison and Optimization of Single-Phase Liquid Cooling Devices for the Heat Dissipation of High-Power LED Arrays. *Applied Thermal Engineering* 59(1–2): 648–59.

Ran, J., L. Li, X. Du, R. Wang, W. Pan and W. Tang (2015). Numerical Investigations on Characteristics of Methane Catalytic Combustion in Micro-Channels with a Concave or Convex Wall Cavity. Energy Conversion and Management 97, 188–95.

Robles, A., V. Doung, A. J. Martin, J. L. Guadarrama and G. Diaz (2014). Aluminum Minichannel Solar Water Heater Performance under Year-Round Weather Conditions. *Solar Energy* 110, 356–64.

Sakamatapan, K. and S. Wongwises. (2014). Pressure Drop during Condensation of R134a Flowing inside a Multiport Minichannel. *International Journal of Heat and Mass Transfer* 75, 31–39.

Sturgis, J. C. and I. Mudawar (1999). Assessment of CHF Enhancement Mechanisms in a Curved, Rectangular Channel Subjected to Concave Heating. *Journal of Heat Transfer* 121(2), 394–404.

Teng, J. (2012). Fluid Dynamics in Microchannels. *Intechopen* 403–36.

Tuo H., Hrnjak P. (2013). Effect of the header pressure drop induced flow maldistribution on the microchannel evaporator performance. *International Journal of Refrigeration* 36(8), 2176–2186.

Tuckerman, D. B. and R. F. W. Pease (1981). High-Performance Heat Sinking for VLSI. *IEEE Electron Device Letters* 2(5), 126–29.

Wajs, J., D. Mikielewicz and E. Fornalik-Wajs (2016). Thermal Performance of a Prototype Plate Heat Exchanger with Minichannels under Boiling Conditions. *Journal of Physics: Conference Series* 745, 032063.

Wang, J. (2011). Theory of Flow Distribution in Manifolds. *Chemical Engineering Journal* 168(3), 1331–45.

Wen, J., and Y. Li. (2004). Study of Flow Distribution and Its Improvement on the Header of Plate-Fin Heat Exchanger. *Cryogenics* 44(11), 823–31.

Zhou, J., X. Zhao, X. Ma, Z. Du, Y. Fan, Y. Cheng and X. Zhang (2017). Clear-Days Operational Performance of a Hybrid Experimental Space Heating System Employing the Novel Mini-Channel Solar Thermal & PV/T Panels and a Heat Pump. *Solar Energy* 155, 464–77.

Zhou, P., D. Tarlet, M. Wei, Y. Fan and L. Luo (2017). Novel Multi-Scale Parallel Mini-Channel Contactor for Monodisperse Water-in-

Oil Emulsification. *Chemical Engineering Research and Design* 121, 233–44.

Zhou, W., W. Deng, L. Lu, J. Zhang, L. Qin, S. Ma and Y. Tang (2014). Laser Micro-Milling of Microchannel on Copper Sheet as Catalyst Support Used in Microreactor for Hydrogen Production. *International Journal of Hydrogen Energy* 39(10), 4884–94.